IEEE Access
Multidisciplinary | Rapid Review | Open Access Journal

Received September 23, 2019, accepted October 11, 2019, date of publication October 28, 2019, date of current version November 8, 2019.

*Digital Object Identifier 10.1109/ACCESS.2019.2949799*

# Crop Area Identification Based on Time Series EVI2 and Sparse Representation Approach: A Case Study in Shandong Province, China

**LAN XUN[1,2,3], JIAHUA ZHANG[1,2,3], DAN CAO[1,2,3], SHA ZHANG[2,4], AND FENGMEI YAO[3]**

[1]Aerospace Information Research Institute, Chinese Academy of Sciences, Beijing 100094, China
[2]Key Laboratory of Digital Earth Science, Institute of Remote Sensing and Digital Earth, Chinese Academy of Sciences, Beijing 100094, China
[3]College of Earth and Planetary Sciences, University of Chinese Academy of Sciences, Beijing 100049, China
[4]Remote Sensing Information and Digital Earth Center, College of Computer Science and Technology, Qingdao University, Qingdao 266071, China

Corresponding author: Jiahua Zhang (zhangjh@radi.ac.cn)

This work was supported in part by the Key Basic Research Project of Shandong Natural Science Foundation of China under Grant ZR2017ZB0422, in part by the Shangdong Key Research and Development Project under Grant 2018GNC110025, in part by the "Taishan Scholar" Project of Shandong Province under Grant TSXZ201712, and in part by the Natural Science Foundation of China under Grant 31671585 and Grant 41871253.

**ABSTRACT** The accurate and timely spatial distribution information of various crop types is vital for food security. In this study, the 2-band enhanced vegetation index (EVI2) data from Moderate Resolution Imaging Spectroradiometer (MODIS) were combined with sparse representation approach to identify the distribution of various crop types in Shandong Province, China. Three groups of input variables derived from EVI2 including annual time series EVI2 (TS), harmonic features (HF), and combined vector formed by harmonic features and texture features (HFT) were used. The online dictionary learning and orthogonal matching pursuit algorithms were applied to generate the dictionary and solve the sparse coefficients of the identified samples, respectively. Then, the label of the identified samples can be obtained according to the minimum residuals between the dictionary and the sparse coefficients of the identified samples. At the provincial level, the validation based on the statistical data showed that three groups of input variables presented lower than $\pm 25\%$ at relative errors, and input variables of HFT performed better than the other two. At the municipal level, the results achieved by using input variables of HFT also agreed well with the statistics with the coefficient of determination $R^2 > 0.85$ for wheat and maize, as well as $R^2 > 0.71$ for peanut and cotton during 2014-2016. These results demonstrate that the combination of the input variables of HFT derived from time series MODIS EVI2 data and sparse representation approach can be used for crop identification in the study area.

**INDEX TERMS** Crop area identification, harmonic features, sparse representation, texture features, time series EVI2.

## I. INTRODUCTION

Crop area identification is of great significance for crop production [1]. The estimation of crop cultivated area is crucial for yield estimation, policymaking, and adjustment of crop planting structures [2], [3]. The traditional methods for obtaining the information of crop cultivated area are based on manual measurement and statistical sampling, which are time-consuming and labor-intensive [4]. Remotely sensed data are an obvious and promising source of information for crop mapping and for monitoring the land cover changes at the regional or global scales [5]–[7].

Previous studies have used the differences of spectral, phenological, and spatial features from remotely sensed data for crop classification [8]–[10]. The implementation of information on the phenology of crops derived from multi-temporal images into the classification process introduces possibilities for crop classification [11]–[14]. The phenological features derived from time series Moderate Resolution Imaging Spectroradiometer (MODIS) data have shown good performance in crop classification [15], [16]. At present, vegetation indices such as normalized difference vegetation index (NDVI)

The associate editor coordinating the review of this manuscript and approving it for publication was Lian Feng.

and enhanced vegetation index (EVI) have been widely applied for vegetation phenology studies [17], [18]. Skakun *et al*. [7] applied a Gaussian mixture model (GMM) to discriminate winter crops from other crops using time series MODIS NDVI and growing degree days (GDD) information. Zhang *et al*. [4] estimated the maize cultivated area in Northeast China using time series MODIS EVI data integrated with crop phenological information, and the overall classification accuracy reached 79%. The development of EVI is aimed to reduce the effect that NDVI can saturate at high leaf area index while minimizing soil and atmosphere influences, which is more suitable for vegetation growth monitoring [19]. However, EVI is limited to sensor systems designed with a blue band, in addition to the red and near-infrared bands, making it limited to generate time series EVI using sensors without a blue band. Therefore, a 2-band enhanced vegetation index (EVI2) without a blue band developed and evaluated by Jiang *et al*. [20] was used in this study, which has the best similarity with the EVI and has been successfully utilized in crop area identification and yield estimation [21], [22].

In recent years, sparse representation has shown promising performance in many applications, such as face recognition [23], target detection [24], image fusion [25], image compression [26], image classification [27], and others [28]. From the theory of sparse representation, an identified sample is assumed to be approximately represented by a linear combination of as few atoms as possible of a given dictionary. The sparse representation-based classifier is more robust to the effect of noise [29]. Taking remote sensing image scene classification as an example, the results from Zhao *et al*. [30] showed that sparse representation-based classifiers can obtain satisfactory results without high feature dimensions, and perform better than linear support vector machine and random forest classifiers. Among the existing studies, sparse representation-based methods have also shown impressive performance in hyperspectral image classification. Both results from Yu *et al*. [31] and Yuan *et al*. [32] showed that sparse representation-based classifiers generally performed better than support vector machine. However, little emphasis has been placed on crop classification by combining time series data and sparse representation approach.

Several studies have been carried out for crop classification by integrating both spectral and spatial information and achieved better effects [33]. Spatial features are often used as auxiliary features in crop classification, with the assumption that neighboring pixels tend to belong to the same class [34]. The implementation of spatial features of crop distribution into the classification process introduces further possibilities for improvement of classification performance [35]. The results from Zhang *et al*. [34] showed that combining spectral and textural features for classification achieved the highest overall accuracy of 98.65%. Reshma *et al*. [36] raised the classification accuracy to 98.07% by integrating the vegetation indices along with the spectral and spatial features for classification. The studies mentioned above indicated that the combination of spectral and spatial features was useful for the identification of various crop types. However, little emphasis has been placed on crop mapping by the combination of phenological and spatial information.

Shandong Province is the major agricultural production areas of China where the wheat, maize, peanut, and cotton acreage accounts for about 16%, 9%, 16%, and 14% of the national total of the corresponding crops in 2016, respectively [37]. There is an increasing demand for accurate and objective acquisition of the spatial distribution of these crops, which is of great significance for regional crop production. The spectral and phenological information have been utilized to discriminate the distribution of crops in Shandong Province in the last decade. Li *et al*. [38] applied a decision tree classification model to identify cotton planting area based on the analysis of spectral characteristics of typical objects derived from CBERS01 and HJ1B satellite images in Dingzhuang town, Shandong Province. Guo *et al*. [39] extracted the distribution of winter wheat, maize, and cotton based on the thresholds between the time series MODIS NDVI and the reference time series NDVI in Dezhou, Binzhou, and Dongying city, Shandong Province. However, the studies mentioned above mainly focus on crop area identification at the small scale (town or municipal level). Therefore, this study incorporated the phenological and spatial features with a sparse representation approach to discriminate the distribution of wheat, maize, peanut, and cotton at the provincial level. Because of its high temporal resolution and the fact that it only needs red and near-infrared bands, time series MODIS EVI2 data have been successfully utilized in the detection of crop phenology [40].

The objectives of this study are: (1) to evaluate the feasibility of sparse representation approach for crop area identification based on time series MODIS EVI2 data, (2) to compare the classification accuracies achieved by using three groups of input variables including annual time series EVI2, harmonic features, and texture features, and (3) to present the mapping results in Shandong Province during 2014-2016.

## II. MATERIALS AND METHODS

### A. STUDY AREA

In this study, Shandong Province was selected as the study area (34°22.9' −38°24.01' N, 114°47.5' −122°42.3' E), which located along the east coast of China (Fig. 1). It occupies an area of 15.8 million hectares, 47.8% of which are cropland. There are 17 administrative units at the municipal level during our study period. This region has a warm temperate monsoon climate, having four seasons with a mean annual temperature of 11 – 14 ° and mean annual precipitation of 550 – 950 mm. The difference in temperature between east and west is higher than that between north and south. This region is rich in light resources and its heat conditions can meet the needs of the double cropping system. Wheat, maize, peanut, and cotton are four major crops in the region, accounting for approximately 35%, 29%, 7%, and 4% of the total crop acreage in 2016, respectively [37]. There are

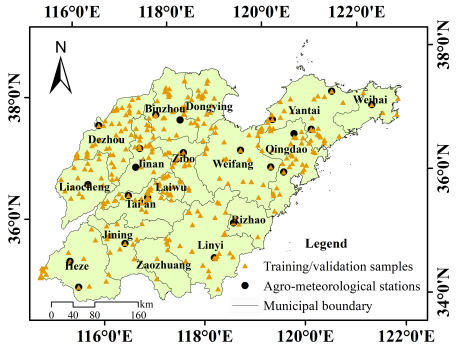


**FIGURE 1.** The spatial distribution of agro-meteorological stations and samples in the study area.

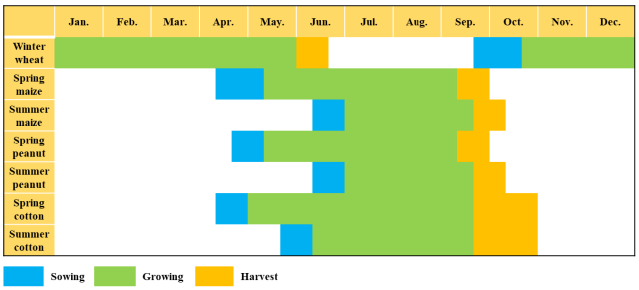


**FIGURE 2.** Crop calendar in the study area.

several big production counties for peanut and cotton, with the planting areas more than 600 hectares.

### B. DATA DESCRIPTION AND PRE-PROCESSING

#### 1) MODIS DATA AND PRE-PROCESSING

The MODIS surface reflectance products (MOD09Q1) for tile h27v05 (h for horizontal, v for vertical) for the years 2014-2016 were obtained from the Land Processes Distributed Active Archive Center (LP DAAC, https://lpdaac.usgs.gov). The temporal resolution of MOD09Q1 is 8 days and spatial resolution is 250 m. The red and near-infrared bands for each compositing period (8 days) were extracted and clipped to the extent of the study area. Then the EVI2 was calculated for each compositing period as follows [20]:

$$\mathrm{EVI2} = 2.5 \times \frac{\rho_{\mathrm{nir}} - \rho_{\mathrm{red}}}{\rho_{\mathrm{nir}} + 2.4 \times \rho_{\mathrm{red}} + 1} \tag{1}$$

where $\rho_{nir}$, $\rho_{red}$ are the reflectance in the near-infrared band (841-876 nm) and red band (620-670 nm), respectively. Annual 46 MODIS EVI2 images were available and the results were stacked for each year.

Additionally, the MODIS land cover type product (MCD12Q1) with a spatial resolution of 500 m was adopted in this study. This product is produced for each calendar year for five different classification schemes. Plant Functional Types (PFT) classification scheme was used in this study to distinguish the cropland from non-cropland areas. More details about the MODIS products are available on the website (https://lpdaac.usgs.gov). The MODIS land cover maps were re-projected to the Lambert Azimuthal Projection and resampled to a spatial resolution of 250 m, enabling us to create a cropland mask for further identification of various crop types.

#### 2) OBSERVATION DATA OF THE AGRO-METEOROLOGICAL STATIONS AND STATISTICAL DATA

The phenology information of crops observed at 22 agro-meteorological stations in Shandong Province were obtained from the National Meteorological Information Center, China Meteorological Administration (http://data.cma.cn/). The locations of these agro-meteorological stations are shown in Fig. 1. Both single cropping (one crop a year) and double cropping (two crops a year) systems are observed in the study area. Double cropping cycles tend to be shorter than single cropping (Fig. 2). In double cropping areas, the first crop (e.g., winter wheat) is planted in September and harvested in June of the following year, whereas the second crop (e.g., summer maize, summer peanut, summer cotton) is planted in May or June and harvested in September. Winter wheat is only planted in the first season, whereas maize, peanut, and cotton are planted in the first or the second seasons around summer. Eventually, winter wheat-summer maize, winter wheat-summer peanut, winter wheat-summer cotton, winter wheat-others, spring maize, spring peanut, spring cotton, and others were selected as the identified types.

Based on the locations of agro-meteorological stations, and the samples from the published papers [41]–[43], the geographical coordinates of samples for different crop types were obtained. Then, combined with crop calendar data, the characteristics of samples shown on Google Earth images and the variation characteristics of annual time series EVI2 of the samples were analyzed. According to Google Earth images and the characteristics of EVI2, such as the number of peak times of EVI2 series, maximum EVI2 values and its occurrence time, and the time with the highest EVI2 increase rates, the samples were supplemented. In total, 418 samples were obtained, as shown in Fig. 1. The number of samples for winter wheat-summer maize, winter wheat-summer peanut, winter wheat-summer cotton, winter wheat-others, spring maize, spring peanut, spring cotton, and others are 108, 16, 30, 32, 24, 28, 26, and 154, respectively. The 50% of the samples were selected as training samples for the generation of the dictionary, and the others preserved for estimating classification accuracy. The statistical cultivated areas data regarding wheat, maize, peanut, and cotton during 2014-2016 at the provincial and municipal level were collected from the Shandong Statistical Yearbook [37]. A summary of the methodological framework employed for classification of the aforementioned crop types in this study is given in Fig. 3, and is described in detail in subsequent sections.

### C. SPARSE REPRESENTATION-BASED CLASSIFICATION

The sparse representation-based classification (SRC) method assumes that the training samples from a single class lie on

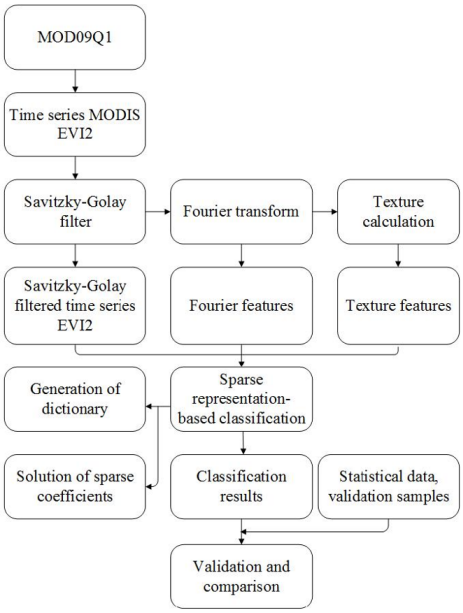


**FIGURE 3.** Flowchart for crop area identification based on time series EVI2 and sparse representation approach.

a subspace [44]. As a result, an identified sample can be represented as a linear combination of the training samples. This representation is sparse when the number of training samples is large enough. According to the sparse representation theory, if an identified sample $\boldsymbol{y}$ belongs to the $m$th class, it could be represented approximately by a linear combination of training samples from the $m$th class as follows [45]:

$$\boldsymbol{y} = \boldsymbol{x}_1^m \boldsymbol{d}_1^m + \boldsymbol{x}_2^m \boldsymbol{d}_2^m + \cdots + \boldsymbol{x}_{N_m}^m \boldsymbol{d}_{N_m}^m = \mathrm{D}^m \boldsymbol{x}^m \tag{2}$$

where $\mathbf{D}^m = \left\{\boldsymbol{d}_j^m\right\}_{j=1,\ldots,N_m} \in \mathbf{R}^{w \times N_m}$ is a sub-dictionary formed by training samples belonging to the $m$th class. $\boldsymbol{d}_j^m \in \mathbf{R}^w$ is a basis vector consisting of $w$ values, which represents a feature column vector of the $j$th training sample from the $m$th class. $w$ denotes the number of input variables. $N_m$ denotes the size of sub-dictionary, representing the number of samples for the $m$th class. $\boldsymbol{x}^m \in \mathbf{R}^{N_m}$ is the sparse coefficients of $\boldsymbol{y}$, and each element in $\boldsymbol{x}^m$ represents the weight of the corresponding atoms in $\mathbf{D}^m$. $\mathbf{R}$ represents a set of real numbers.

Suppose the training dataset consists of $M$ classes, the identified sample $\boldsymbol{y}$ could be in a collection of all the sub-dictionaries of total $M$ classes $\{\mathbf{D}^m\}_{m=1,\ldots,M}$, which can be represented by a sparse coefficient vector $\boldsymbol{x}$ multiplying the dictionary $\mathbf{D}$ as follows:

$$\boldsymbol{y} = \mathbf{D}^1 \boldsymbol{x}^1 + \mathbf{D}^2 \boldsymbol{x}^2 + \cdots + \mathrm{D}^M \boldsymbol{x}^M = \mathbf{D}\boldsymbol{x} \tag{3}$$

where $\mathbf{D} \in \mathbf{R}^{w \times N}$ is the dictionary, containing $N$ training samples for $M$ classes, $N = \sum_{m=1}^{M} N_m$. $\boldsymbol{x} \in \mathbf{R}^N$ is the sparse matrix consisting of $\{\boldsymbol{x}^m\}_{m=1,\ldots,M}$ associated with $\boldsymbol{y}$, where only a few entries are non-zero. Ideally, if $\boldsymbol{y}$ belongs to the $m$th class, $\boldsymbol{x}^j = 0, \forall\ j = 1, \ldots, m,\ j \neq m$. The label of the identified sample $\boldsymbol{y}$ can be obtained based on the above formulation.

### 1) GENERATION OF DICTIONARY

One of the key issues of the SRC method is to obtain an over-completed dictionary that allows the sparse representation of the identified samples to the obtained dictionary, which means that the number of atoms in the dictionary should outweigh the feature dimension of the samples ($N >> w$). In this study, the training samples were used as the input to initialize the dictionary, and the online dictionary learning algorithm [46] was used for the generation of the dictionary. The learning process is explained as follows [47]:

Step 1: Initialize the matrices $\mathrm{A}_0$ and $\mathbf{B}_0$, $\mathbf{A}_0 = \mathbf{O}$ ($\mathbf{A}_0 \in \mathbf{R}^{k \times k}$), $\mathbf{B}_0 = \mathbf{O}$ ($\mathbf{B}_0 \in \mathbf{R}^{w \times k}$). Let $\mathbf{D}_0 \in \mathbf{R}^{w \times N}$ be the initial dictionary to be trained, a matrix consists of the training samples for $M$ classes. Set $\mathbf{D} = \mathbf{D}_0$,$N_m = 200$. Initialize the number of iterations $q$ as 1.

Step 2: The sparse coefficients after the $q$th iteration can be calculated using the least angle regression algorithm [48] as follows:

$$\boldsymbol{x}_q \triangleq \arg\min_{\boldsymbol{x} \in \mathbf{R}^N} \frac{1}{2} \left\|\boldsymbol{y}_q - \mathbf{D}_{q-1}\boldsymbol{x}\right\|_2^2 + \gamma \left\|\boldsymbol{x}\right\|_1 \tag{4}$$

where $\|\cdot\|_2 = \sqrt{\sum_{\eta=1}^{w} \left|\cdot_\eta\right|^2}$ represents the $l_2$-norm, and $\|\boldsymbol{x}\|_1 = \sum_{\eta=1}^{w} \left|\boldsymbol{x}_\eta\right|$ represents the $l_1$-norm. $\gamma \in \mathbf{R}$ represents a regularization parameter, with a value that specifies the compromise between data reconstruction error and sparsity, and is set to 0.15 in this study.

Step 3: Update the dictionary after the $q$th iteration $\mathbf{D}_q$ using the algorithm in [46];

Step 4: Set the max iteration number $q_{max} = 200$. Set $q = q + 1$ when $q < 200$, and repeat steps 2-3 for loop iteration. Exit the iteration when $q = 200$, and $\mathbf{D}_q$ is as requested.

### 2) SOLUTION OF SPARSE COEFFICIENTS

From the theory of sparse representation, given an overall dictionary, the sample $\boldsymbol{y}$ can be represented linearly by a few atoms of the dictionary, and a projection coefficient vector can be obtained as follows [45]:

$$\boldsymbol{x} = \arg\min \left\|\mathrm{D}\boldsymbol{x} - \boldsymbol{y}\right\|_2, \quad s.t. \left\|\boldsymbol{x}\right\|_0 \leq K_0 \tag{5}$$

where $\|\boldsymbol{x}\|_0$ denotes the $l_0$-norm of $\boldsymbol{x}$, representing the number of non-zero entries of the vector. $K_0$ is an upper bound on the sparsity level.

However, the solution of (5) is nondeterministic polynomial-time hard (NP-hard), and it is difficult to approximate in the general case [49]. The orthogonal matching pursuit [50] can be used to solve the problem. This algorithm solves the sparse coefficients $\boldsymbol{x}$ of the identified sample $\boldsymbol{y}$ based on the dictionary $\mathbf{D} = [\mathbf{D}^1\mathbf{D}^2 \ldots \mathbf{D}^M]$, which is assumed as known at first. The detailed description can be found in [50].

#### 3) CATEGORY IDENTIFICATION

Based on the above algorithms, the dictionary $\mathbf{D}$ and sparse coefficients $\boldsymbol{x}$ can be obtained, both of which are used to identify the class label of $\boldsymbol{y}$. Ideally, most of the coefficients in $\boldsymbol{x}$ are zero, whereas few coefficients which correspond to its class-specific sub-dictionary are nonzero. In practice, some coefficients in $\boldsymbol{x}$ corresponding to other class-specific sub-dictionaries are also nonzero because of the effect of noise. The reconstructed residuals on different class-specific sub-dictionaries are usually different. The smaller the residual on the class-specific sub-dictionary, the more likely that the sample belongs to the corresponding class. Thus, $\boldsymbol{y}$ is assigned to the class corresponding to the minimum residual $r^m(\boldsymbol{y})$ as follows [45]:

$$r^m(\boldsymbol{y}) = \left\|\boldsymbol{y} - \mathbf{D}^m\boldsymbol{x}^m\right\|_2, \quad m = 1, 2, \ldots, M \tag{6}$$

$$\text{class}\,(\boldsymbol{y}) = \arg\min_{m=1,2,\ldots,M} r^m(\boldsymbol{y}) \tag{7}$$

The generation of the dictionary, solution of sparse coefficients, and category identification were all implemented using MATLAB software.

### D. GROUPS OF INPUT VARIABLES FOR CLASSIFICATION

Several groups of input variables were developed using time series MODIS EVI2. The classification was performed by using each group of input variables, including: (i) annual time series EVI2 (TS), containing 46 yearly Savitzky-Golay filtered values; (ii) harmonic features (HF), containing the amplitudes of the terms 0-5 and the phases of the terms 1-5 derived from the Fourier transform; (iii) a combined vector formed by the 11 harmonic features and 2 texture features (HFT). Details of data processing procedures for each group are given in the following sections.

#### 1) SAVITZKY-GOLAY FILTER

The annual time series EVI2 derived from MODIS images still include various noise components due to the presence of cloudiness, seasonal snow, instrument problems, and some other problems. Therefore, a data smoothing method needs to be applied to minimize the impact of noise before utilizing time series EVI2 data to reflect the growth status and temporal variation of crops. Compared with other methods such as the best index slope extraction (BISE) [51] and asymmetric Gaussian function fitting method [52], the upper envelope Savitzky-Golay filter is designed to fit the upper envelope and to reflect the changing patterns of the time series data through an iteration process. The main advantage of this method is that it tends to preserve the curve shape features, which is important for crop classification [53]. Therefore, the upper envelope Savitzky–Golay filter was applied to smooth the annual time series EVI2 data. The general equation can be given as follows [54]:

$$\text{EVI2}_t^s = \sum_{h=-g}^{g} \frac{C_h \text{EVI2}_{t+h}^0}{2g+1} \tag{8}$$

where $t$ is an integer with a value ranging from 1 to 46, which corresponds to the compositing periods, 1, 2, …, 46. $g$ is the half-width of moving window to perform filtering, and is set as 2 in this study. $C_h$ is the coefficient, which can be found in [54]. $\text{EVI2}_{t+h}^0$ is the $h$th original EVI2 in the smoothing window. $\text{EVI2}_t^s$ is the filtered data, which is the linear combination of $C_h$ and $\text{EVI2}_{t+h}^0$. In this study, subsequent data processing is based on the filtered data.

#### 2) FEATURE EXTRACTION BASED ON FOURIER TRANSFORM

Statistical techniques that work in the frequency or time domain, such as Fourier transform, have been used to extract information from time series of vegetation index and proved to be suitable in the analysis of the temporal dynamics of vegetation [18]. A time-dependent periodic phenomenon can be decomposed into a series of cosine waves defined by unique amplitude and phase values by Fourier transform, which are correlated with information on crop types. In this study, discrete Fourier transform was employed to process the 46 Savitzky-Golay filtered EVI2 ($\text{EVI2}_t^s$) in a year as follows [55]:

$$F_z = \frac{1}{46}\sum_{t=0}^{45} \text{EVI2}_t^s \exp\left(-\frac{2\pi izt}{46}\right) \tag{9}$$

where $F_z$ is the $z$th Fourier coefficient, $z$ =0, 1, 2 …45, and $\text{i}^2 = -1$. Amplitude and phase can be calculated according to $F_z$. Based on the previous work [47], the amplitudes of the terms 0-5 and the phases of the terms 1-5 derived from the Fourier transform were used as the feature vector for crop identification.

#### 3) FEATURE EXTRACTION BASED ON TEXTURE ANALYSIS

The detailed structures of ground objects can be represented by texture effectively. It reflects the repeated occurrence of image grayscale without depending on the color and brightness of ground objects, which is a common internal feature of all surface features. Various methods have been reported to extract the texture feature from the image. The grey level co-occurrence matrix (GLCM), one of the best-known spatial and textural feature analysis methods for images, provides information about the joint distribution of two pixels through spatial correlation analysis of the grey levels of the image [56]. Therefore, the entropy of the GLCM was used for crop area identification in this study, which is one of the widely-used textural features for image classification [57]. The amplitude of the term 0 derived from the Fourier transform represents the mean value of the time series data, accounting for a large percentage of the total variance in the time series data. The phase of term 1 defines the offset between the original time series data and the peak of the first wave over the range 0 to $2\pi$ [58]. Therefore, the entropy values for both the amplitude of the term 0 and the phase of the term 1 were obtained using ENVI software. The expression for entropy (H) is given as follows [56]:

$$\text{H} = -\sum_u \sum_v c(u, v) \log\left(c(u, v)\right) \tag{10}$$

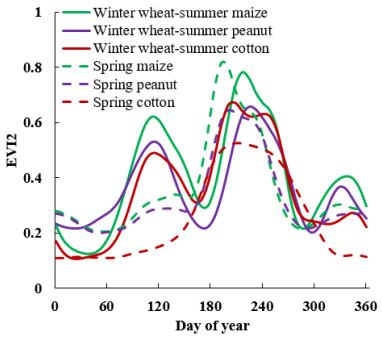


**FIGURE 4.** The time series EVI2 for main crop types in the study area.

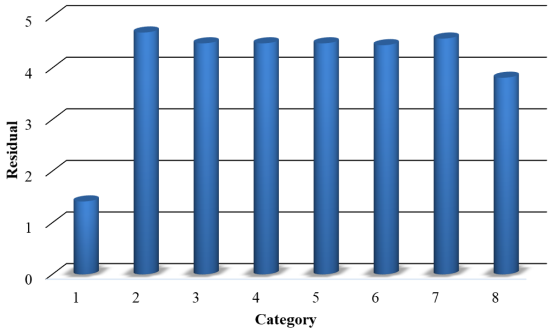


**FIGURE 5.** Residual value map of a test sample of winter wheat-summer maize. The numbers 1-8 correspond to winter wheat-summer maize, winter wheat-summer peanut, winter wheat-summer cotton, winter wheat-others, spring maize, spring peanut, spring cotton, and others, respectively.

where $c(u, v)$ is the element of GLCM, $u$ and $v$ represent the row and column elements of the matrix, respectively.

## III. RESULTS AND DISCUSSION

### A. ANALYSIS OF TIME SERIES EVI2

The annual time series EVI2 for main crop types are shown in Fig. 4. The results showed that there were two significant peaks of the time series EVI2 in double cropping areas. Also, there was a small peak around November, which corresponds to the tillering stage of winter wheat. There was one significant peak of the time series EVI2 in single cropping areas including spring maize, spring peanut, and spring cotton. The peak of the time series EVI2 for cotton maintained for a longer time than other crops. The peak occurrence time of the time series EVI2 for maize and peanut in single cropping areas were earlier than those in double cropping areas.

### B. THE RESIDUALS OF DIFFERENT CLASS

Based on the dictionary and sparse coefficients, the residuals of identified samples were calculated. Taking a test sample of winter wheat-summer maize as an example, the residual value map corresponding to each category is shown in Fig. 5. The horizontal axis indicates the category of training samples, and the vertical axis is the residual of the test sample corresponding to each category. The result showed that the residual corresponding to the sub-dictionary of winter wheat-summer maize was minimal. It indicated that the test sample was predicted to belong to winter wheat-summer maize. That is to say, the test sample is correctly assigned to the class which has the minimum residual.

### C. CLASSIFICATION ACCURACY ANALYSIS

#### 1) COMPARISON OF CLASSIFICATION ACCURACIES USING THREE GROUPS OF INPUT VARIABLES

The classification experiments were conducted using the SRC method with three groups of input variables, respectively. The distribution of various crop types in the study area is shown in Fig. 6. To assess and compare the accuracies of classification results achieved by using three groups of input variables, validation samples of each type in 2016 were used for confusion matrix calculation. The user's accuracy (UA), producer's accuracy (PA), and overall accuracy (OA) were calculated (Table 1). The results showed that the overall accuracies of 3 classification results varied between 76.56% and 80.86%, which were acceptable accuracies for crop identification. The overall accuracy of classification results achieved by using input variables of HFT was the highest, followed by using input variables of HF, and the lowest by using input variables of TS. For three groups of the input variable, user's and producer's accuracies achieved by using input variables of HFT were much higher than those by the other two groups of input variables, except for spring maize, spring cotton, and others. Compared with the results achieved by using input variables of TS, user's and producer's accuracies achieved by using input variables of HF were much higher for winter wheat-summer peanut, winter wheat-others, and spring maize. Compared with the results achieved by using input variables of HF, we observed that adding texture features for classification resulted in an increased in user's accuracy except for spring maize and others, as well as increased of

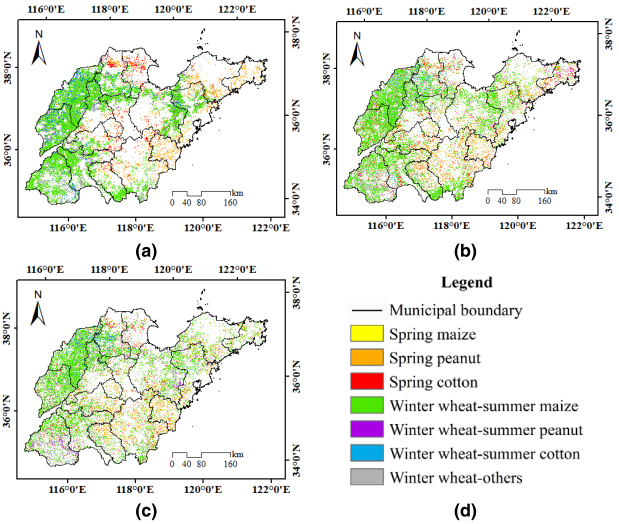


**FIGURE 6.** Spatial distribution of crop types in Shandong Province in 2016 using three groups of input variables: (a) TS, (b) HF, and (c) HFT. (d) is the legend.

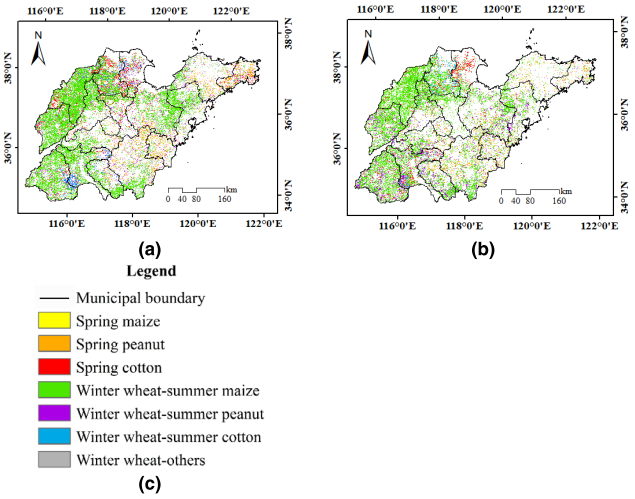


**FIGURE 7.** Spatial distribution of crop types in Shandong Province using the SRC method with input variables of HFT in the years of (a) 2014 and (b) 2015. (c) is the legend.

**TABLE 1.** Comparison of classification accuracies achieved by using three groups of input variables in 2016.

| Crop types | Input variables | | | | | |
|---|---|---|---|---|---|---|
| | TS | | HF | | HFT | |
| | UA(%) | PA (%) | UA(%) | PA (%) | UA (%) | PA (%) |
| WM | 83.33 | 74.07 | 82.35 | 77.78 | 86.54 | 83.33 |
| WP | 71.43 | 62.50 | 85.71 | 75.00 | 85.71 | 75.00 |
| WC | 71.43 | 66.67 | 61.11 | 73.33 | 83.33 | 66.67 |
| WO | 66.67 | 62.50 | 68.75 | 68.75 | 75.00 | 75.00 |
| M | 80.00 | 66.67 | 81.82 | 75.00 | 69.23 | 75.00 |
| P | 66.67 | 71.43 | 81.82 | 64.29 | 84.62 | 78.57 |
| C | 75.00 | 69.23 | 61.54 | 61.54 | 68.75 | 84.62 |
| O | 77.27 | 88.31 | 81.71 | 87.01 | 81.25 | 84.42 |
| OA(%) | 76.56 | | 77.99 | | 80.86 | |

Note: WM, WP, WC, WO, M, P, C, O represent winter wheat-summer maize, winter wheat-summer peanut, winter wheat-summer cotton, winter wheat-others, spring maize, spring peanut, spring cotton, and others, respectively.

producer's accuracy except for winter wheat-summer cotton and others. This indicated that texture features derived from MODIS image with the spatial resolution of 250 m can improve the performance in classification and detection, which is consistent with [59].

Moreover, the MODIS-derived results were compared with official statistical results at the provincial level. The relative errors for the four crops were calculated as shown in Table 2. The results indicated that three groups of input variables presented lower than ±25% at relative errors, and the input variables of HFT presented lower than 15% at relative errors. The estimated areas obtained using three groups of input variables were all overestimated in different degree, except for maize area obtained using input variables of HFT. The phenological characteristics of crops led to the variation of different growth stages and different types of vegetation have different seasonal rhythms, which can be reflected in time series vegetation index data [4]. The 46 annual time series EVI2 values were used as input variables for crop area

**TABLE 2.** Relative errors of four crops using three groups of input variables at the provincial level in 2016.

| Crop | Relative error using input variables (%) | | |
|---|---|---|---|
| | TS | HF | HFT |
| Wheat | 18 | 15 | 2 |
| Maize | 13 | 10 | -3 |
| Peanut | 17 | 16 | 15 |
| Cotton | 25 | 22 | 11 |

identification and presented lower than 25% at relative errors for four crops. Compared with this group of input variables, the 11 harmonic features performed better, presenting lower than 22% at relative errors. Compared with the input variables of TS, the input variables of HF is more efficient at saving the storage space and improving the recognition rate in data processing. The main features of time series data can be reflected in the first few harmonic features so that the noise can be further removed. Furthermore, when texture features were added for classification, the classification result produced the lowest relative errors. Thus, the texture features have shown their effectiveness in crop classification. This effect is especially noticeable for the classification accuracies of wheat and maize. The probable reason is that the planting areas of wheat and maize are relatively larger than other crops in the study area and the spatial distribution is more continuous. Moreover, the classification accuracy of cotton has also been greatly improved compared with the other 2 groups of input variables. Compared with the input variables of HF, both phenological and spatial features of crops were considered when using the input variables of HFT during the classification process.

The relative errors of wheat and maize obtained using three groups of input variables were smaller than those for peanut and cotton. One of the potential sources that cause errors in the results is the effect of mixed pixels. In some areas, the fields of peanut and cotton are relatively small compared with the 250 m MODIS cell size so that the areas for peanut and cotton may be overestimated. Moreover, the characteristics of the key growth stage reflected in the time series EVI2 of part samples for peanut and cotton are similar to each other. Thus the relative errors of these two crops are not higher than the other two crops using the SRC method based on different groups of input variables.

### 2) ANALYSIS OF CLASSIFICATION ACCURACY DURING 2014-2016

The distribution maps of wheat, maize, peanut, and cotton during 2014-2015 were obtained using the SRC method with the input variables of HFT (Fig. 7). At the municipal level, a comparison between estimated and statistical crop areas during 2014-2016 was performed, and the coefficient of determination ($R^2$) was calculated (Fig. 8). The results showed that the $R^2$ reached 0.85 for wheat and maize, and it reached 0.71 for peanut and cotton. The corresponding points stay closer to 1:1 line as shown in Fig. 8(a) and (b) than those

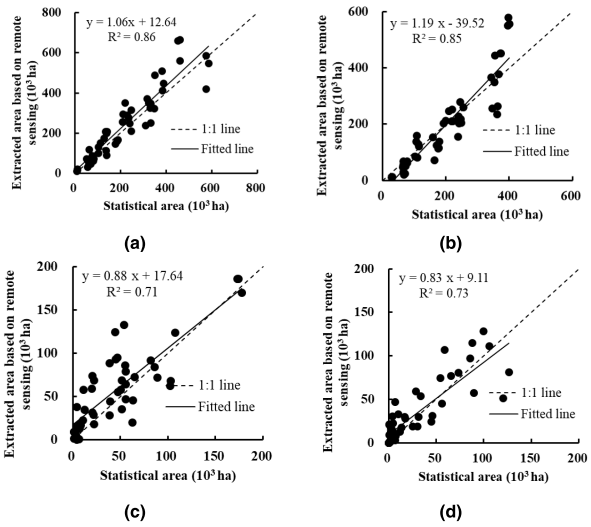


**FIGURE 8. Comparison between MODIS-derived area with input variables of HFT and statistical data at the municipal level during 2014-2016. (a)-(d) represent wheat, maize, peanut, and cotton, respectively.**

in Fig. 8(c) and (d). The slopes of the linear fitted line for the four crops were between 0.83 and 1.19. These results showed that using both harmonic features and texture features derived from time series EVI2 as well as SRC method for multi-year crop identification was feasible and stable.

There are some points that need to be noted in the classification process. First, the classification accuracy of the method used in this study mainly depends on the differences in the features between the identified samples and training samples of multiple crop types in the dictionary. As wheat is only planted in the first season in the study area, which is usually from September to June of the following year, with fewer crops planted at the similar growing seasons. It is easier to discriminate winter wheat from other crops because the differences of both harmonic and texture features between winter wheat and other crop types are obvious. As a result, winter wheat planting areas were well identified with a higher $R^2$ of 0.86 and a slope of the linear fitted line of 1.06 as shown in Fig. 8(a). There are multiple autumn harvest crops in the study area, such as maize, peanut, cotton, soybean, etc. The planting areas of maize are relatively larger and more continuous than other autumn harvest crops planted at the same time. As a result, the texture features of maize planting area are easier to distinguish than those of other crops. The classification accuracy of maize was much higher with $R^2$ of 0.85 and slope of the linear fitted line of 1.19 as shown in Fig. 8(b). The classification accuracies of peanut and cotton were much lower, with $R^2$ of 0.71 and 0.73, respectively.

Second, one of the potential sources that cause errors in the MODIS-derived results is pixel purity. Although high-spatial-resolution datasets such as Landsat have advantages for capturing the fine spatial details of the land cover, such datasets do not have high temporal coverage frequency over large regions and are often affected by extensive cloud cover. Coarse-resolution sensors such as MODIS provide data at a near-daily observational coverage frequency and over large areas. However, in some areas where cropland is relatively fragmented, mixed pixels containing different ground objects might cause uncertainties in the classification results. This might lead to the non-identification of broken cropland. Therefore, the problem incurred by mixed pixels of MODIS data need to be addressed in future work to improve the classification accuracy, e.g., decomposition of the mixed pixel, fusion of Landsat 8, Sentinel 2, and MODIS data.

Third, in this study, the spatial accuracy of classification results was assessed by validation samples, which were obtained partly from the published papers and supplemented based on phenology features of various crops. More field survey data should also be adopted in further research. Moreover, the MODIS land cover type product was used in this study to distinguish croplands from non-croplands, which maybe result in the errors of the MCD12Q1 product being propagate into the mapping results. Also, another potential source that caused errors in the MODIS-derived results is the differences in crop growth conditions in various fields influenced by sowing dates, management measures, and other factors.

### D. DISTRIBUTION OF CROP PLANTING AREAS OVER STUDY AREA

The spatial distribution of crops in the MODIS-derived results is consistent with the general patterns of crop cultivation over the study area (Fig. 6(c), Fig. 7). Single cropping and double cropping systems were the main crop patterns in the study area. First season winter wheat followed by second season summer maize was the dominant double cropping system, and the spatial distribution was relatively continuous. The distribution of winter wheat-summer maize was largely concentrated in the northwest part of Shandong Province. The planting areas of winter wheat-summer peanut, winter wheat-summer cotton, and winter wheat-others were relatively small. The planting patterns of peanut and cotton were dominated by single cropping system, supplemented by rotation or relay cropping with winter wheat.

The spatial distribution of peanut and cotton was relatively dispersed. The planting areas of cotton and peanut showed a decreasing trend from 2014 to 2016. Cotton planting areas in Dongying and Heze city were relatively concentrated during 2014-2015. It can be observed that the planting areas of winter wheat-summer cotton in Heze city were relatively concentrated in 2014. The planting areas of peanut were mainly distributed in the central and southern parts of Shandong Province. It is consistent with the fact that there are the largest peanut planting areas in Linyi city of Shandong Province during 2014-2016. Moreover, crop planting areas in the central and eastern parts of Shandong Province were relatively sparse due to the influences of topography and climate.

### E. PARAMETER ANALYSIS

To evaluate the influences of parameters in the SRC method, correlation analysis between statistical data and

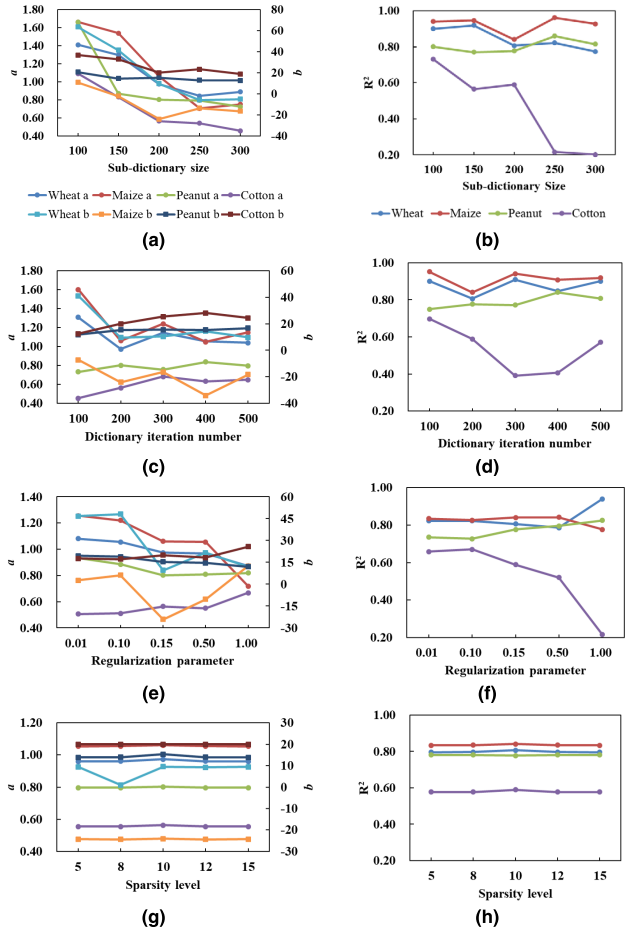


**FIGURE 9.** **Comparison of classification accuracy with different parameter settings including sub-dictionary size, dictionary iteration number, regularization parameter, and sparsity level. (a), (c), (e), and (g) represent *a*, *b* values with different parameter settings, respectively; (b), (d), (f), and (h) represent $R^2$ values with different parameter settings, respectively.**

MODIS-derived area achieved by using input variables of HFT with different parameters were performed at the municipal level in 2016. The values of slope ($a$), intercept ($b$), and $R^2$ were calculated for the four crops with different parameter settings, respectively, and were used to evaluate the classification performance. The basic parameter settings are sub-dictionary size ($N_m$) of 200, dictionary iteration number ($q_{\max}$) of 200, regularization parameter ($\gamma$) of 0.15, and sparsity level ($K_0$) of 10. The $a$,$b$, and $R^2$ values corresponding to the results of a certain varying parameter based on the basic parameter settings are shown in Fig. 9. The $R^2$ values of wheat, maize, and peanut with different parameters including sub-dictionary size, dictionary iteration number, regularization parameter, and sparsity level were higher than 0.77, 0.77, and 0.72, respectively. The $R^2$ values of cotton were relative lower with obvious change as the change of the four parameters. The more effective method for cotton mapping will be our future work. Among the four parameters, it can be observed that $a$, $b$, and $R^2$ values were stable with varying sparsity level as shown in Fig. 9 (g)-(h). The sub-dictionary size, dictionary iteration number, and regularization parameter have greater influences than the sparsity level on the final results, since they determine the dictionary for category identification. As shown in Fig. 9 (a), with the sub-dictionary size increasing, the $a$ and $b$ values showed a decreasing trend around $a = 1$ and $b = 0$, respectively. This indicated that the MODIS-derived area showed a trend from overestimation to underestimation.

Fig. 9 (b) indicates that it is not always performed well with larger sub-dictionary size, especially for cotton. Therefore, the default parameter setting for the sub-dictionary size was set to 200 with the full consideration of the optimum $a$, $b$, and $R^2$ values. Fig. 9 (c)-(d) illustrate that with the dictionary iteration number changing, the $a$, $b$, and $R^2$ values show the fluctuating tendency. Although the $R^2$ values for four crops except peanut obtained using the dictionary iteration number of 100 were better than those with the dictionary iteration number of 200, the $a$ and $b$ values for the former were relatively poor. Therefore, $q_{\max} = 200$ was set as the default parameters setting. Also, the $a$ and $b$ values obtained using the regularization parameter of 1.00 were much better than those with the regularization parameter of 0.15 as shown in Fig. 9 (e), whereas the $R^2$ values for the latter was comparatively higher with full consideration of four crops as shown in Fig. 9 (f). Therefore, the regularization parameter of 0.15 is a good choice in this study.

## IV. CONCLUSION

The accurate spatial distribution information of crops is important for national food security. In this study, combined with time series MODIS EVI2 data, the SRC method was successfully implemented for the identification of wheat, maize, peanut, and cotton in Shandong Province. At the provincial level, the results achieved by using input variables of HFT presented lower than $\pm 15\%$ at relative errors and performed better than those by using the input variables of TS and HF. At the municipal level, the results showed that the cultivated area estimated from MODIS were well correlated with the statistical data with $R^2 > 0.85$ for wheat and maize as well as $R^2 > 0.71$ for peanut and cotton during 2014-2016. It indicated a robust potential of combining phenological and texture information for crop identification. Resultant maps presented consistent patterns for the spatial distribution of crops across multiple years. Besides, there are different effects on the results with varying parameter settings using the sparse representation approach. The sparsity level has little influence on the final results, whereas sub-dictionary size, dictionary iteration number, and regularization parameter have obvious effects on the performance since they influence the generation of dictionary for category identification. Of course, there are still many challenges in crop area identification while considering the variety of cropping systems, including management practices and field sizes. Further research could also explore to improve the classification accuracy by fusion of Landsat 8, Sentinel 2, and MODIS data.

## REFERENCES

[1] Y. Cai, K. Guan, J. Peng, S. Wang, C. Seifert, B. Wardlow, and Z. Li, "A high-performance and in-season classification system of field-level crop types using time-series Landsat data and a machine learning approach," *Remote Sens. Environ.*, vol. 210, pp. 35–47, Jun. 2018.

[2] K. Jia, Q. Li, Y. Tian, B. Wu, F. Zhang, and J. Meng, "Crop classification using multi-configuration SAR data in the North China plain," *Int. J. Remote Sens.*, vol. 33, no. 1, pp. 170–183, 2012.

[3] R. Sonobe, Y. Yamaya, H. Tani, X. Wang, N. Kobayashi, and K.-I. Mochizuki, "Assessing the suitability of data from sentinel-1A and 2A for crop classification," *GISci. Remote Sens.*, vol. 54, no. 6, pp. 918–938, 2017.

[4] J. Zhang, L. Feng, and F. Yao, "Improved maize cultivated area estimation over a large scale combining MODIS–EVI time series data and crop phenological information," *ISPRS J. Photogramm. Remote Sens.*, vol. 94, pp. 102–113, Aug. 2014.

[5] J. D. Wickham, S. V. Stehman, J. H. Smith, and C. G. Homer, "Thematic accuracy of the NLCD 2001 land cover for the conterminous United States," *Remote Sens. Environ.*, vol. 114, no. 6, pp. 1286–1296, 2001.

[6] Y. Zha, Y. Liu, and X. Deng, "A landscape approach to quantifying land cover changes in Yulin, Northwest China," *Environ. Monit. Assessment*, vol. 138, nos. 1–3, pp. 139–147, 2008.

[7] S. Skakun, B. Franch, E. Vermote, J.-C. Roger, I. Becker-Reshef, C. Justice, and N. Kussul, "Early season large-area winter crop mapping using MODIS NDVI data, growing degree days information and a Gaussian mixture model," *Remote Sens. Environ.*, vol. 195, pp. 244–258, Jun. 2017.

[8] C. Conrad, R. R. Colditz, S. Dech, D. Klein, and P. L. G. Vlek, "Temporal segmentation of MODIS time series for improving crop classification in Central Asian irrigation systems," *Int. J. Remote Sens.*, vol. 32, no. 23, pp. 8763–8778, 2011.

[9] Y. Pan, L. Li, J. Zhang, S. Liang, X. Zhu, and D. Sulla-Menashe, "Winter wheat area estimation from MODIS-EVI time series data using the crop proportion phenology index," *Remote Sens. Environ.*, vol. 119, pp. 232–242, Apr. 2012.

[10] Y. Zhou, X. Xiao, Y. Qin, J. Dong, G. Zhang, W. Kou, C. Jin, J. Wang, and X. Li, "Mapping paddy rice planting area in rice-wetland coexistent areas through analysis of Landsat 8 OLI and MODIS images," *Int. J. Appl. Earth Observ. Geoinf.*, vol. 46, pp. 1–12, Apr. 2016.

[11] L. Zhong, L. Hu, L. Yu, P. Gong, and G. S. Biging, "Automated mapping of soybean and corn using phenology," *ISPRS J. Photogramm. Remote Sens.*, vol. 119, pp. 151–164, Sep. 2016.

[12] D. Bargiel, "A new method for crop classification combining time series of radar images and crop phenology information," *Remote Sens. Environ.*, vol. 198, pp. 369–383, Sep. 2017.

[13] S. Hariharan, D. Mandal, S. Tirodkar, V. Kumar, A. Bhattacharya, and J. M. Lopez-Sanchez, "A novel phenology based feature subset selection technique using random forest for multitemporal PolSAR crop classification," *IEEE J. Sel. Topics Appl. Earth Observ. Remote Sens.*, vol. 11, no. 11, pp. 4244–4258, Nov. 2018.

[14] M. Belgiu and O. Csillik, "Sentinel-2 cropland mapping using pixel-based and object-based time-weighted dynamic time warping analysis," *Remote Sens. Environ.*, vol. 204, pp. 509–523, Jan. 2018.

[15] K. Jia, S. Liang, X. Wei, Y. Yao, Y. Su, B. Jiang, and X. Wang, "Land cover classification of landsat data with phenological features extracted from time series MODIS NDVI data," *Remote Sens.*, vol. 6, no. 11, pp. 11518–11532, 2014.

[16] P. Hao, Y. Zhan, L. Wang, Z. Niu, and M. Shakir, "Feature selection of time series MODIS data for early crop classification using random forest: A case study in Kansas, USA," *Remote Sens.*, vol. 7, no. 5, pp. 5347–5369, 2015.

[17] Y. Zha, J. Gao, S. Ni, Y. Liu, J. Jiang, and Y. Wei, "A spectral reflectance-based approach to quantification of grassland cover from Landsat TM imagery," *Remote Sens. Environ.*, vol. 87, nos. 2–3, pp. 371–375, 2003.

[18] A. Moreira, D. C. Fontana, and T. M. Kuplich, "Wavelet approach applied to EVI/MODIS time series and meteorological data," *ISPRS J. Photogramm. Remote Sens.*, vol. 147, pp. 335–344, Jan. 2019.

[19] A. R. Huete, K. Didan, T. Miura, E. P. Rodriguez, X. Gao, and L. G. Ferreira, "Overview of the radiometric and biophysical performance of the MODIS vegetation indices," *Remote Sens. Environ.*, vol. 83, nos. 1–2, pp. 195–213, 2002.

[20] Z. Jiang, A. R. Huete, K. Didan, and T. Miura, "Development of a two-band enhanced vegetation index without a blue band," *Remote Sens. Environ.*, vol. 112, no. 10, pp. 3833–3845, 2008.

[21] H. Sun, A. Xu, H. Lin, L. Zhang, and Y. Mei, "Winter wheat mapping using temporal signatures of MODIS vegetation index data," *Int. J. Remote Sens.*, vol. 33, no. 16, pp. 5026–5042, 2012.

[22] D. K. Bolton and M. A. Friedl, "Forecasting crop yield using remotely sensed vegetation indices and crop phenology metrics," *Agricult. Forest Meteorol.*, vol. 173, pp. 74–84, May 2013.

[23] Y. Gao, J. Ma, and A. L. Yuille, "Semi-supervised sparse representation based classification for face recognition with insufficient labeled samples," *IEEE Trans. Image Process.*, vol. 26, no. 5, pp. 2545–2560, May 2017.

[24] Y. Zhang, B. Du, and L. Zhang, "A sparse representation-based binary hypothesis model for target detection in hyperspectral images," *IEEE Trans. Geosci. Remote Sens.*, vol. 53, no. 3, pp. 1346–1354, Mar. 2015.

[25] F. Fakhari, M. R. Mosavi, and M. M. Lajvardi, "Image fusion based on multi-scale transform and sparse representation: An image energy approach," *IET Image Process.*, vol. 11, no. 11, pp. 1041–1049, Jul. 2017.

[26] J.-C. Ni, Q. Zhang, Y. Luo, and L. Sun, "Compressed sensing SAR imaging based on centralized sparse representation," *IEEE Sensors J.*, vol. 18, no. 12, pp. 4920–4932, Jun. 2018.

[27] Y. Shao, N. Sang, and C. Gao, "Spatial and class structure regularized sparse representation graph for semi-supervised hyperspectral image classification," *Pattern Recognit.*, vol. 81, pp. 81–94, Sep. 2018.

[28] C. Wu, B. Du, and L. Zhang, "Hyperspectral anomalous change detection based on joint sparse representation," *ISPRS J. Photogramm. Remote Sens.*, vol. 146, pp. 137–150, Dec. 2018.

[29] T. Jin, X. Hou, P. Li, and F. Zhou, "A novel method of automatic plant species identification using sparse representation of leaf tooth features," *PLoS ONE*, vol. 10, no. 10, 2015, Art. no. 0139482.

[30] L. Zhao and P. Tang, "Scalability analysis of typical remote sensing data classification methods: A case of remote sensing image scene," *J. Remote Sens.*, vol. 20, no. 2, pp. 157–171, 2016.

[31] H. Yu, L. Gao, W. Li, Q. Du, and B. Zhang, "Locality sensitive discriminant analysis for group sparse representation-based hyperspectral imagery classification," *IEEE Geosci. Remote Sens. Lett.*, vol. 14, no. 8, pp. 1358–1362, Aug. 2017.

[32] H. Yuan and Y. Y. Tang, "Sparse representation based on set-to-set distance for hyperspectral image classification," *IEEE J. Sel. Topics Appl. Earth Observ. Remote Sens.*, vol. 8, no. 6, pp. 2464–2472, Jun. 2015.

[33] L. Zhang, L. Zhang, D. Tao, and X. Huang, "On combining multiple features for hyperspectral remote sensing image classification," *IEEE Trans. Geosci. Remote Sens.*, vol. 50, no. 3, pp. 879–893, Mar. 2012.

[34] X. Zhang, Y. Sun, K. Shang, L. Zhang, and S. Wang, "Crop classification based on feature band set construction and object-oriented approach using hyperspectral images," *IEEE J. Sel. Topics Appl. Earth Observ. Remote Sens.*, vol. 9, no. 9, pp. 4117–4128, Sep. 2016.

[35] Y. Jin, X. Liu, Y. Chen, and X. Liang, "Land-cover mapping using random forest classification and incorporating NDVI time-series and texture: A case study of central Shandong," *Int. J. Remote Sens.*, vol. 39, no. 23, pp. 8703–8723, 2018.

[36] S. Reshma, S. Veni, and J. E. George, "Hyperspectral crop classification using fusion of spectral, spatial features and vegetation indices: Approach to the big data challenge," in *Proc. Int. Conf. Adv. Comput. Commun. Inform. (ICACCI)*, Sep. 2017, pp. 380–386.

[37] *Shandong Provincial Bureau of Statistical, Shandong Statistical Yearbook*, China Statist. Press, Beijing, China, 2017.

[38] M. Li, G. Zhao, and Y. Qin, "Extraction and monitoring of cotton area and growth information using remote sensing at small scale: A case study in Dingzhuang town of Guangrao County, China," in *Proc. Int. Conf. Comput. Distrib. Control Intell. Environ. Monit. (CDCIEM)*, Feb. 2011, pp. 816–823.

[39] Y. S. Guo, Q. S. Liu, G. H. Liu, and C. Huang, "Extraction of main crops in yellow river delta based on MODIS NDVI time series," *J. Nature Resour.*, vol. 32, no. 10, pp. 1808–1818, 2017.

[40] X. Zhang and Q. Zhang, "Monitoring interannual variation in global crop yield using long-term AVHRR and MODIS observations," *ISPRS J. Photogramm. Remote Sens.*, vol. 114, pp. 191–205, Apr. 2016.

[41] M. M. Cui, K. R. Wang, L. L. Wang, and Y. X. Shi, "Distribution characteristics of phthalic acid esters in soils and peanut kernels in main peanut producing areas of Shandong Province, China," *Chin. J. Appl. Ecol.*, vol. 24, no. 12, pp. 3523–3530, 2013.

[42] J. Dai, Z. Luo, W. Li, W. Tang, D. Zhang, H. Lu, Z. Li, C. Xin, X. Kong, A. E. Eneji, and H. Dong, "A simplified pruning method for profitable cotton production in the Yellow River valley of China," *Field Crops Res.*, vol. 164, pp. 22–29, Aug. 2014.

[43] W. He, F. Han, R. Guan, G. Wang, H. Wang, Y. Lou, F. Song, and Y. Zhuge, "Effects of different fertilization models on nitrogen, phosphorus accumulation and yield of cotton in coastal saline-alkali soil," *J. Soil Water Conserv.*, vol. 32, no. 3, pp. 295–300, 2018.
[44] J. Wright, A. Y. Yang, A. Ganesh, S. S. Sastry, and Y. Ma, "Robust face recognition via sparse representation," *IEEE Trans. Pattern Anal. Mach. Intell.*, vol. 31, no. 2, pp. 210–227, Feb. 2009.
[45] Y. Chen, N. M. Nasrabadi, and T. D. Tran, "Hyperspectral image classification using dictionary-based sparse representation," *IEEE Trans. Geosci. Remote Sens.*, vol. 49, no. 10, pp. 3973–3985, Oct. 2011.
[46] J. Mairal, F. Bach, J. Ponce, and G. Sapiro, "Online learning for matrix factorization and sparse coding," *J. Mach. Learn. Res.*, vol. 11, pp. 19–60, Mar. 2010.
[47] L. Xun, P. Wang, L. Li, L. Wang, and Q. Kong, "Identifying crop planting areas using Fourier-transformed feature of time series MODIS leaf area index and sparse-representation-based classification in the North China plain," *Int. J. Remote Sens.*, vol. 40, nos. 5–6, pp. 2034–2052, 2018.
[48] B. Efron, T. Hastie, I. Johnstone, and R. Tibshirani, "Least angle regression," *Ann. Statist.*, vol. 32, no. 2, pp. 407–451, 2004.
[49] E. Amaldi and V. Kann, "On the approximability of minimizing nonzero variables or unsatisfied relations in linear systems," *Theor. Comput. Sci.*, vol. 209, nos. 1–2, pp. 237–260, 1998.
[50] J. A. Tropp and A. C. Gilbert, "Signal recovery from random measurements via orthogonal matching pursuit," *IEEE Trans. Inf. Theory*, vol. 53, no. 12, pp. 4655–4666, Dec. 2007.
[51] N. Viovy, O. Arino, and A. S. Belward, "The best index slope extraction (BISE): A method for reducing noise in NDVI time-series," *Int. J. Remote Sens.*, vol. 13, no. 8, pp. 1585–1590, 1992.
[52] P. Jonsson and L. Eklundh, "Seasonality extraction by function fitting to time-series of satellite sensor data," *IEEE Trans Geosci. Remote Sens.*, vol. 40, no. 8, pp. 1824–1832, Aug. 2002.
[53] J. Chen, P. Jönsson, M. Tamura, Z. Gu, B. Matsushita, and L. Eklundh, "A simple method for reconstructing a high-quality NDVI time-series data set based on the Savitzky–Golay filter," *Remote Sens. Environ.*, vol. 91, nos. 3–4, pp. 332–344, 2004.
[54] A. Savitzky and M. J. E. Golay, "Smoothing and differentiation of data by simplified least squares procedures," *Anal. Chem.*, vol. 36, no. 8, pp. 1627–1639, 1964.
[55] M. Zhang, Q. Zhou, Z. Chen, J. Liu, Y. Zhou, and C. Cai, "Crop discrimination in Northern China with double cropping systems using Fourier analysis of time-series MODIS data," *Int. J. Appl. Earth Observ. Geoinf.*, vol. 10, no. 4, pp. 476–485, 2008.
[56] R. M. Haralick, K. Shanmugam, and I. Dinstein, "Textural features for image classification," , vol. SMC-3, no. 6, pp. 610–621, Nov. 1973.
[57] H. Zhang, Q. Li, J. Liu, J. Shang, X. Du, H. McNairn, C. Champagne, T. Dong, and M. Liu, "Image classification using RapidEye data: Integration of spectral and textual features in a random forest classifier," *IEEE J. Sel. Topics Appl. Earth Observ. Remote Sens.*, vol. 10, no. 12, pp. 5334–5349, Dec. 2017.
[58] M. E. Jakubauskas, D. R. Legates, and J. H. Kastens, "Harmonic analysis of time-series AVHRR NDVI data," *Photogramm. Eng. Remote Sens.*, vol. 67, no. 4, pp. 461–470, 2001.
[59] H. Su, Y. Wang, J. Xiao, and L. Li, "Improving MODIS sea ice detectability using gray level co-occurrence matrix texture analysis method: A case study in the Bohai Sea," *ISPRS J. Photogramm. Remote Sens.*, vol. 85, pp. 13–20, Nov. 2013.

**LAN XUN** received the B.S. degree in geographic information systems from Shanxi Agricultural University, Jinzhong, China, in 2016, and the M.S. degree in cartography and geographical information systems from China Agricultural University, Beijing, China, in 2018. She is currently pursuing the Ph.D. degree with the Institute of Remote Sensing and Digital Earth, Chinese Academy of Sciences, Beijing. Her main research interest includes the application of remote sensing in crop classification.

**JIAHUA ZHANG** received the Ph.D. degree in cartography and remote sensing from the Institute of Remote Sensing Applications, Chinese Academy of Sciences (CAS), in 1998. From 1999 to 2001, he held a postdoctoral position at the National Institute for Environmental Studies, Japan. Since 2002, he has been a Professor with the Chinese Academy of Meteorological Sciences. Since 2012, he has been a Full Professor with the Institute of Remote Sensing and Digital Earth, CAS. His research interests include global climate change and disaster remote sensing, atmospheric environment, land use, and vegetation dynamic. He has published more than 150 peer review articles, 30 international conferences papers, and six books.

**DAN CAO** received the B.S. and M.S. degrees from Henan Polytechnic University, in 2015 and 2018, respectively. She is currently pursuing the Ph.D. degree with the Institute of Remote Sensing and Digital Earth, Chinese Academy of Sciences, Beijing, China. She is mainly engaged in the expertise area of agriculture remote sensing and vegetation change research.

**SHA ZHANG** received the B.S. degree from the College of Resource and Environmental Sciences, Hebei Normal University, in 2011, the M.S. degree from the College of Resource and Environmental Sciences, Hebei Normal University, in 2015, and the Ph.D. degree from the Institute of Remote Sensing and Digital Earth, Chinese Academy of Sciences, in 2019. She is currently holding a full-time postdoctoral position with Qingdao University. Her interested areas include crop mapping with remote sensing, crop yield estimation, and terrestrial ecosystem productivity simulation.

**FENGMEI YAO** received the Ph.D. degree in meteorology from the Institute of Atmospheric Physics, Chinese Academy of Sciences (CAS), Beijing, China, in 2005. Since August 2005, she has been an Assistant Professor with the Graduated University of Chinese Academy of Sciences. Since 2017, she has been a Full Professor with the College of Earth and Planetary Sciences, University of Chinese Academy of Sciences. She has been involved in climate change and effect on vegetation and agriculture, atmospheric environment, and disaster. She has published more than 100 peer-reviewed articles, 20 international conferences papers, and four books.